Eur. Phys. J. Special Topics **171**, 37–43 (2009)

DOI: 10.1140/epjst/e2009-01009-7

THE EUROPEAN PHYSICAL JOURNAL SPECIAL TOPICS

Regular Article

Application of the multi distribution function lattice Boltzmann approach to thermal flows

A. Parmigiani[1,a], C. Huber[2], B. Chopard[1], J. Latt[3], and O. Bachmann[4]

[1] Computer Science Department, University of Geneva, 24 rue du Général Dufour, 1211 Geneva 4, Switzerland
[2] Department of Earth and Planetary Science, University of California – Berkeley, 307 McCone Hall 4767, Berkeley, CA 94720-4767, USA
[3] Department of Mathematics, Tufts University, 503 Boston Avenue, Medford, MA 02155, USA
[4] Department of Earth and Space Science, University of Washington, Johnson Hall, Seattle, WA 98195-1310, USA

Abstract. Numerical methods able to model high Rayleigh (Ra) and high Prandtl (Pr) number thermal convection are important to study large-scale geophysical phenomena occuring in very viscous fluids such as magma chamber dynamics ($10^4 < Pr < 10^7$ and $10^7 < Ra < 10^{11}$). The important variable to quantify the thermal state of a convective fluid is a generalized dimensionless heat transfer coefficient (the Nusselt number) whose measure indicates the relative efficiency of the thermal convection. In this paper we test the ability of Multi-distribution Function approach (MDF) Thermal Lattice Boltzmann method to study the well-established scaling result for the Nusselt number ($Nu \propto Ra^{1/3}$) in Rayleigh Bénard convection for $10^4 \leq Ra \leq 10^9$ and $10^1 \leq Pr \leq 10^4$. We explore its main drawbacks in the range of Pr and Ra number under investigation: (1) high computational time N_c required for the algorithm to converge and (2) high spatial accuracy needed to resolve the thickness of thermal plumes and both thermal and velocity boundary layer. We try to decrease the computational demands of the method using a multiscale approach based on the implicit dependence of the Pr number on the relaxation time, the spatial and temporal resolution characteristic of the MDF thermal model.

1 Introduction

Over the last two decades the Lattice Boltzmann method (LB), has demonstrated its versatility for modeling the behavior of flows in complex geometries [12], involving phase transitions [6] and multiple fluids [7]. The simplicity and locality of LB methods offers a powerful alternative to standard CFD methods to model complex geophysical flows.

The Lattice Boltzmann method has been already applied to Rayleigh Benard Convection (RBC), however, to our knowledge, RBC at high Pr and Ra, has been scarcely investigated with LB models [1,8]. Owing to the limited range over which the relaxation times for each distributions are stable and accurate, the Pr is often limited to 10^{-1} to 10^1.

In this paper we study RBC for an isoviscous fluid using the Multi Distribution Function LB approach (MDF) [8,9]. We test the model over a large range of Prandtl and Rayleigh number ($10^1 \leq Pr \leq 10^4$, $10^4 \leq Ra \leq 10^9$) finding an increasing demand of computational requirements with increasing Pr and Ra. We try to decrease the computational requirements making use of

[a] e-mail: andrea.parmigiani@unige.ch

two multiscale strategies. These methods arise from the definition of Pr which is based on the set of free parameters that the MDF model offers to tune the transport coefficients (viscosity ν and thermal diffusivity κ). We investigate the advantages and drawbacks of this approach.

2 Rayleigh-Benard convection

Rayleigh Benard convection, an example of natural convection, occurs when buoyancy forces due to thermal expansion of an isoviscous fluid exceeds viscous forces [14]. The set of dimensionless equations describing RBC for a Boussinesq fluid can be written as:

$$\nabla \cdot \mathbf{u}^* = 0, \tag{1}$$

$$\frac{\partial \mathbf{u}^*}{\partial t} + \mathbf{u}^* \cdot (\nabla \cdot \mathbf{u}^*) = -\frac{\nabla p^*}{\rho_0^*} + \sqrt{\frac{Pr}{Ra}} \nabla^2 \mathbf{u}^* - T^* \mathbf{z}, \tag{2}$$

$$\frac{\partial T^*}{\partial t} + \mathbf{u}^* \cdot \nabla \mathbf{T}^* = \sqrt{\frac{1}{PrRa}} \nabla^2 T^*. \tag{3}$$

In the above equations the scaling for temperature $T^* = (T - T_0)/(T_h - T_c)$, velocity $\mathbf{u}^* = (t_0/H)\mathbf{u}$ and dynamic pressure $p^*/\rho_0^* = pt_0^2/\rho l_0^2$ are used (upper-index $*$ indicates dimensionless units), where T_h and T_c are the top and bottom temperature, $t_0 = \sqrt{H/g_0\beta(T_h - T_c)}$ and H are the characteristic time and length of the system, ρ_0^* is the dimensionless density at the reference temperature $T_0 = (T_h + T_c)/2$ and $\mathbf{z}$ the direction of gravity g_0. The Prandtl and the Rayleigh numbers are defined respectively as $Pr = \nu/\kappa$ and $Ra = g_0\beta(T_h - T_c)H^3/(\kappa\nu)$ where β is the thermal expansion, ν is the viscosity of the fluid, κ is its thermal diffusivity. From linear stability analysis we expect a power-law relationship between Nusselt (Nu), defined as convective divided by conductive heat transfer, and Ra numbers [14]. In this work we use, as a benchmark for our code, the well established relation [5]

$$Nu = 1.46(Ra/Ra_{cr})^{0.281}. \tag{4}$$

It is of fundamental importance for our work to underline that from experiments and boundary layer theory [15], we know that the characteristic size of both thermal plumes, velocity and thermal boundary layers decrease for increasing Pr and Ra number. For more details on the different regimes of convection observed over these range of Ra and Pr, we refer the reader to [2,4].

3 The multi distribution function approach

In the MDF LB approach [8,9] applied to thermal problems, the fluid and the temperature field are respectively described by two different particle distribution functions

$$f_i = f_i(\mathbf{x}, \mathrm{t}), \quad \mathrm{i} = 0, \ldots, \mathrm{M}, \qquad \mathrm{g_i} = \mathrm{g_i}(\mathbf{x}, \mathrm{t}), \quad \mathrm{i} = 0, \ldots, \mathrm{K} \tag{5}$$

where $\mathbf{x}$ is the position on the lattice at the time t and i the index of the discrete set of velocity directions connecting the lattice node $\mathbf{x}$ with its neighbors.

Density ρ^+, momentum $\rho^+\mathbf{u}^+$ and temperature T^+ of the fluid (the upperscript $+$ indicates LB units) can be calculated at each lattice node:

$$\rho^+ = \sum_{i=0}^{M} f_i, \quad \rho^+\mathbf{u}^+ = \sum_{i=1}^{M} f_i\,\mathbf{e}_i, \quad T^+ = \sum_{i=0}^{K} g_i, \tag{6}$$

where $\mathbf{e}_i$ is the local particle velocity for the f_i lattice. It is important to underline that in the MDF approach the only exchange of information between the particle distribution functions is through the macroscopic quantities, therefore M and K can assume different values. In other

words we could think of the MDF method as two different numerical schemes, used for the evaluation of f_i and g_i respectively, which are eventually coupled. This statement helps us to understand that not only different velocity directions can be used in the two numerical schemes, but also different size grids δx and time steps δt.

For modeling two dimensional RBC we use the D2Q9 ($M=8$) lattice [12] for f_i and the D2Q5 ($K=4$) lattice [10] for g_i. Corresponding lattice velocities (e_i,v_i) and weights(w_i^F, w_i^T) for the two topologies are:

- D2Q9: $e_0 = (0,0), e_1 = (1,0), e_2 = (0,1), e_3 = (1,0), e_4 = (0,1), e_5 = (1,1), e_6 = (1,1)$, $e_7 = (1,1)$ and $e_8 = (1,1)$ with weights $w_0^F = 4/9, w_1^F = w_2^F = w_3^F = w_4^F = 1/9$ and $w_5^F = w_6^F = w_7^F = w_8^F = 1/36$;
- D2Q5: $v_0 = (0,0), v_1 = (1,0), v_2 = (0,1), v_3 = (1,0), v_4 = (0,1)$ with weights $w_0^T = 1/3$, $w_1^T = w_2^T = w_3^T = w_4^T = 1/6$.

In this work we use a LBGK approximation [12,13] to calculate the evolution of f_i and g_i:

$$f_i(\mathbf{x}+\mathbf{e}_i, t+1) = f_i(\mathbf{x},t) - \frac{1}{\tau_F}(f_i(\mathbf{x},t) - f_i^{eq}(\mathbf{x},t)) + \mathbf{e}_i \cdot \mathbf{F_z}; \tag{7}$$

$$g_i(\mathbf{x}+\mathbf{v}_i, t+1) = g_i(\mathbf{x},t) - \frac{1}{\tau_T}(g_i(\mathbf{x},t) - g_i^{eq}(\mathbf{x},t)); \tag{8}$$

where:

$$F_z = \rho_0^+ w_i^F \frac{(T^+ - T_0^+)}{T_h^+ - T_c^+} \frac{\delta t_F^2}{\delta x_F} \mathbf{z}. \tag{9}$$

The force term F_z describes the buoyancy force, due to thermal expansion of the fluid, responsible of driving the flow.

In eqs. 7, τ_F and τ_T are the relaxation time. The equilibrium distributions for the $D2Q9$ and the $D2Q5$ lattices are given by

$$f_i^{eq} = \rho^+ w_i^F \left[1 + 3(\mathbf{e}_i \cdot \mathbf{u}^+) + \frac{9}{2}(\mathbf{e}_\mathrm{i} \cdot \mathbf{u}^+)^2 - \frac{3}{2}\mathbf{u}^+ \cdot \mathbf{u}^+\right], \tag{10}$$

$$g_i^{eq} = T^+ w_i^T \left[1 + \frac{1}{3}(\mathbf{v}_i \cdot \mathbf{u}^+)\right]. \tag{11}$$

Through a Chapman-Enskog procedure, we can recover the system of eqs. 1, 2 and 3. We define the time and spatial scales of the problem by

$$\delta t_F = \frac{N^*}{N_F}, \quad \delta t_T = \frac{N^*}{N_T}, \quad \delta x_F = \frac{H^*}{H_F - 1}, \quad \delta x_T = \frac{H^*}{H_T - 1}, \tag{12}$$

where the indices F and T refer respectively to the fluid and temperature lattice discretizations; H_F and H_T are the number of lattice nodes used to discretize a reference length H^* for the two grids, while N_F and N_T are the number of iterations used for the simulation of a reference laps of time N^* (we choose to set $H^* = N^* = 1$). We can relate the transport coefficients of the model in lattice units (ν^+ and κ^+) to Pr and Ra by

$$\nu^+ = \frac{1}{3}(\tau_F - 0.5) = \sqrt{\frac{Pr}{Ra}} \frac{\delta t_F}{\delta x_F^2}, \quad \kappa^+ = \frac{1}{3}(\tau_T - 0.5) = \sqrt{\frac{1}{PrRa}} \frac{\delta t_T}{\delta x_T^2}. \tag{13}$$

For stability consistency τ_F and τ_T have to be larger than 0.5. Using eqs. 13 we can derive an expression for Pr in terms of relaxation times, grid spacing and timesteps for the two distributions:

$$Pr = \frac{\tau_F - 0.5}{\tau_T - 0.5} \frac{\delta x_F^2}{\delta x_T^2} \frac{\delta t_T}{\delta t_F}. \tag{14}$$

When different time and spatial scales for f_i and g_i are used, the macroscopic velocity calculated for the f_i distribution has to be rescaled in the system of units of the thermal scheme by

$$u_T^+ = \frac{\delta t_T}{\delta t_F} \frac{\delta x_F}{\delta x_T} u_F^+. \tag{15}$$

For each run, we set Pr, Ra, the size of the grids (H_k where $k = F, T$), the relaxation time τ_F and, through eq. 13, we find δt_F. Once the ratio between δt_F and δt_T is chosen, we derive τ_T from eq. 14.

4 Three different ways to set the *Pr* number, the full coupling and the decoupling methods

In the MDF thermal approach, velocity and temperature evolution can be thought as two independent LB schemes which are coupled after collision and streaming steps using the macroscopic temperature T^+ and velocity $\mathbf{u_F^+}$. From our point of view, to play with different time and spatial scales for the two schemes means to reduce the coupling. One of the goal of this paper is to investigate how much the decoupling can be stressed and how it can help to decrease the time of computation required for the solution to converge. We tune the decoupling of the two schemes using the definition of Pr given in eq. 14. This eq. shows that we have three degrees of freedom for setting the Pr number. These degrees of freedom are given by the ratios of the six free parameters of the model τ_F, τ_T, δx_F, δx_T, δt_F and δt_T. In this section, we discuss how to make use of the different free parameters to set the Pr number of our simulations and what the different methods imply in terms of coupling.

1. Relaxation times, full coupling. Assuming $\delta x_F = \delta x_T$ and $\delta t_F = \delta t_T$, we recover the classical MDF approach to set Pr with the ratio of the relaxation times of the two distributions. This method doesn't imply any decoupling process because time and spatial scale are equal for the two numerical schemes. For accuracy reasons we fix $\tau_F = 1$; as a consequence we use τ_T as a free parameter to increase Pr. In order to reach $Pr \gg 1$, we need to set τ_T close to its lower theoretical bound (0.5).

2. Different timestep duration for the two distributions, time decoupling. The second way to increase Pr is to choose $\delta t_T > \delta t_F$. We investigate this method using $\delta x_F = \delta x_T$ and fixing the values of both τ_F and τ_T. From the computational point of view, this means that the evolution of the temperature distribution g_i has to be computed once every $\delta t_T/\delta t_F$ iterations of the scheme for f_i and thus we decrease the time of computation. However, this is done at the expense of stability of the model. In this case, the Pr number can be thought as the product of two terms $Pr = Pr_\tau R$, where $Pr_\tau = (\tau_F - 0.5)/(\tau_T - 0.5)$ and $R = \delta t_T/\delta t_F$. We call R the decoupling time parameter.

3. Different grid spacing for the two distributions, spatial decoupling. Lastly, Pr can be increased by choosing $\delta x_F > \delta x_T$ (i.e. $N_F < N_T$). In other words, a coarser grid for the velocity scheme, would help us to increase the Pr number decreasing the time of computation. Because u^+ and T^+ have to be known at each node of the two lattices, an interpolation step is required. However, if the two grids are properly overlaped, only u_F^+ needs to be interpolated. In our scheme we use an inverse weighting interpolation method [11], where the interpolated quantity of interest is averaged on the neighborhood. For each lattice node belonging to the bulk of the g_i grid, the interpolated and rescaled velocity u_T^+ is calculated as

$$u_T^+ = \left(\frac{\sum_i^X \dfrac{u_F^+}{d_{i,j}}}{\sum_i^X \dfrac{1}{d_{i,j}}} \right) \left(\frac{\delta x_F}{\delta x_T} \right), \tag{16}$$

where X is the number of lattice nodes belonging to the f_i grid that are involved in the calculation of u_T^+ and $d_{i,j}$ is the distance between the node j of g_i grid and the node i of the f_i grid. We call $\delta x_F/\delta x_T$ the decoupling space parameter.

5 Discussion: Limits of the methods

In this section we test the stability and efficiency of the three methods and we focus our attention on the well-studied relation $Nu = 1.46(Ra/Ra_{cr})^{0.281}$. As Ra increases, the transition from steady to unsteady state occurs and the Nu number becomes time-dependent. However, it has been showed numerically and experimentally [3,4] that averaging the Nu over a large enough period of time, leads to a good agreement with eq. 4.

Fig. 1a shows the results for the first method ($\tau_F \neq \tau_T$, $\delta x_F = \delta x_T, \delta t_F = \delta t_F$). We tested the scaling relationship for $Nu(Ra)$ for a wide variety of Ra and $Pr = 10, 100, 1000$. In these calculations, in order to reach high Ra and Pr, the relaxation time τ_T has to be set to values close to 0.5 ($\tau_T = 0.505$ and 0.5005 for $Pr = 100$ and 1000 respectively) but it does not seem to introduce any numerical instability. The results clearly show that Nu is independent of Pr as expected from the scaling law. However, we observe a change in the power-law exponent for $Ra/Ra_c \geq 10^2$ that we attribute to a too small resolution of the thermal δ_T and velocity δ_F boundary layers. In order to verify this hypothesis in a more quantitative way, we made three numerical experiments with $Ra = 3 * 10^6$, $Pr = 100$ and N_F equal to 100,200,400; the found Nu numbers are equal to 10.8, 11.3 and 11.6, where the expected vale is equal to 11.9. Of course better numerical accuracy is reached at the expense of higher computational requirements.

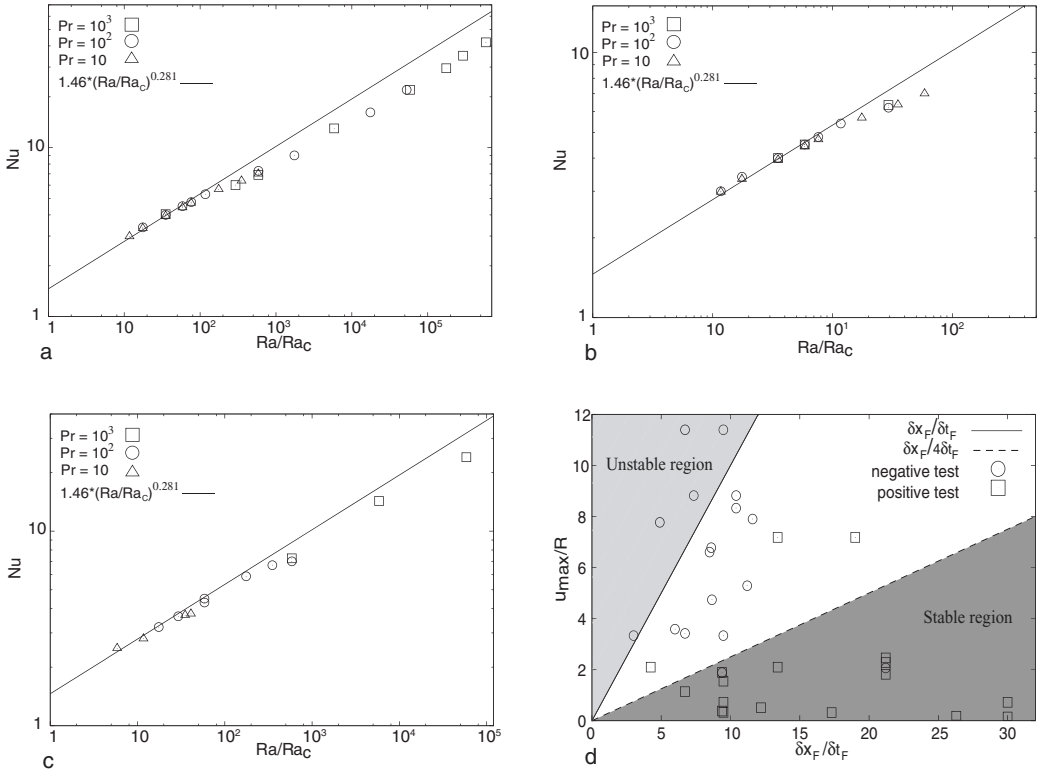

Fig. 1. In fig. a, b, c, we report respectively the ratio Ra/Ra_{cr} on x axes and the Nu number on the y axes. We compare the expected Na-Ra relation 4 (solid line) with the numerical results obtained with the different methods: (a) full coupling , (b) time decoupling and (c) spatial decoupling respectively. In all the graphs, runs for $Pr = 10, 100, 1000$ are reported. In graph b, $R = 1, 10, 100$ for $Pr = 10, 100, 100$. In graph c, $\delta x_F = 4\delta x_T$ for $Ra/Ra_{cr} < 1000$ and $\delta x_F = 2\delta x_T$ for $Ra/Ra_{cr} < 1000$. X is equal to 4. In fig. d, we report stable (square) and unstable (circle) simulations where the value of Pr is determined using the decoupling method. On the x axes we report $\delta x_F/\delta t_F$. The graph is divided into three regions: $u_{max}/R > \delta x_F/\delta t_F$ (unstable region), $u_{max}/R < \delta x_F/4\delta t_F$ (stable region) and the unpredictable region confined between $\delta x_F/4\delta t_F < u_{max}/R < \delta x_F/\delta t_F$.

Fig. 1b shows the comparison between the results and the scaling law for fixed relaxation times ($\tau_F = 1, \tau_T = 0.55$ and different time scales for f_i and g_i. The experiments are conducted for $Pr = 10, 100, 1000$ with $R = 1, 10, 100$ respectively ($R = \delta t_T / \delta t_F$). The bigger the R, the higher the decoupling between the two numerical schemes. In the investigated range of Pr and Ra, the stability of the method allows us to reach $(Ra/Ra_{cr}) = 300$ (Nu is already time-dependent). The impossibility to use further the time decoupling method shows that the higher the Ra number, the stronger the coupling between the two numerical schemes. This fact is not surprising; looking at eq. 1, we can notice that to increase Pr and Ra means to push the heat transport to become velocity controlled and prevent the decoupling of the two schemes. From a numerical point of view we have to avoid a too big temporal variation of the temperature on a given lattice node. Hence R must decrease. On the other hand, for the working region of the method, the accuracy is comparable to the first one. For a more quantitative idea of the stability of time decoupling method, we look for a Courant type stability condition. We impose that the characteristic maximum velocity of the fluid flow (u_{max}) has to be such that $u_{max}\delta t_T \leq \delta x_F$. Using the relation $Re = u_{max}H/\nu \sim Pr^{-1}Ra^{2/3}$, the stability condition can be rewritten as

$$c\frac{\nu^+}{H_F}Pr_\tau^{-1}Ra^{2/3} \leq \frac{\delta x_F}{\delta t_F} \tag{17}$$

where the definition of $Pr = Pr_\tau R$ has been used and c is a constant that has to be determined. From linear stability analysis (at Ra close to Ra_c) the constant in equation 17 is expected to be $c = 0.27$. However, we are interested in a range of Ra far from Ra_c and then we expect a smaller value of c. Fig. 1d shows stable (squares) and unstable (circle) simulations in terms of the stability criterion of eq. 17. The numerical experiments are conducted in a wide range of Ra and $Pr (Ra \leq 10^9, 10^1 \leq Pr \leq 10^4)$. We call stable region, the shaded part of the graph below the straight line with slope equal to $1/4$, our chosen value of c. The time decoupling method improves a lot the efficiency of the algorithm when it can be used. For example when $R = 100$ the temperature scheme is almost negligible.

Finally, for the third method, using different grids size for f_i and g_i seems to be an efficient way to increase the Pr number as $Pr \sim (\delta x_F/\delta x_T)^2$. On the other hand, this method has to be used carefully for the following reasons: at high Ra and Pr (1) high ratios $\delta x_F/\delta x_T$ require higher order of interpolation (computationally more demanding), (2) the thickness of the boundary layers and the plumes (δ) is narrow compared to the size of the system ($\delta/H \sim Ra^{-1/3}$). Thus, in order to resolve the flow, we need $\delta x_F < \delta$; however, large Pr numbers require $N_T > N_F$. This requirement leads to large computational costs and confine the efficiency of the spatial decoupling method only at relative small Ra and high Pr numbers. In this last case, the use of a coarse grid for the f_i scheme can help us to double or quadruple the δt of the simulation and, consequently, to speed it up. Fig. 1c shows the scaling law and the numerical results obtained using two different grid spacing for the two distributions for $Pr = 10, 100, 1000$. For experiments with $Ra/Ra_{cr} < 1000$, $\delta x_F = 4\delta x_T$ and $X = 4$ neighbors for the interpolation (eq. 16). For $Ra/Ra_{cr} > 1000$, a ratio of $\delta x_F = 2\delta x_T$ has been used. We can notice that for a well chosen decoupling space parameter, the accuracy of the results does not change significantly.

6 Conclusions

The Multi Distribution Function approach is a valid and versatile technique for modeling thermal fluids flows over a wide range of Ra and Pr. In this work we explored a wide region of Pr and Ra numbers ($10^1 \leq Pr \leq 10^4, 10^4 \leq Ra \leq 10^9$) for the Rayleigh Benard convection problem. Unfortunately, the classical MDF method, which uses the same grid for both g_i and f_i schemes, is computationally demanding at high Pr and Ra numbers. Therefore we propose different multiscale strategies (decoupling methods) to model high Ra and Pr convection in order to try to decrease the time of computation. These methods consist of (1) to play with a separation of timescales between the thermal (g_i) and fluid (f_i) distribution functions by updating g_i every R iterations of f_i ($R > 1$ for $Pr > 1$). This method proves to be very efficient computationally, however it is limited by a Courant-type condition to an upper bound

of $Ra \sim 300 Ra_c$. The second method (2) is based on to use two different spatial resolutions for the two distributions. In order to increase Pr, the grid spacing of g_i needs to be smaller than the grid spacing for f_i. This method is the most stable, however it is limited by the need to resolve the boundary layer thickness δ. The different methods can be used together (see eq. 14) for more efficiency. However both decoupling methods shows that for high Pr and Ra numbers, when the heat transport becomes velocity controlled, the possibility to decouple the two schemes is reduced.

We would like to thank Michael Manga for helpful comments and Orestis Malaspinas for the stimulating discussions. This work was mainly supported by the FNRS and partially supported by École Doctorale Suisse Romande the Minéralogie (EDSM).

References

1. F. Massaioli, R. Benzi, S. Succi, Europhys. Lett. **21**, 305 (1993)
2. U.R. Christensen, Geophys. Res. Lett. **14**, 220 (1987)
3. U. Hansen, D.A. Yuen, S.E. Kroening, Phys. Fluids A **2**, 2157 (1990)
4. M. Manga, D. Weeraratne, Phys. Fluids **11**, 2969 (1999)
5. F.M. Richter, H. Nataf, S.F. Daly, J. Fluid Mech. **129**, 173 (1983)
6. C. Huber, A. Parmigiani, B. Chopard, M. Manga, O. Bachmann, Int. J. Heat Fluid Flow (in press)
7. X. Shan, S. Chen, Phys. Rev. E **47**, 1815 (1993)
8. X. Shan, Phys. Rev. E **55**, 2780 (1997)
9. Z. Guo, B. Shi, C. Zheng, Int. J. Num. Meth. Fluids **39**, 325 (2002)
10. S. Suga, Int. J. Mod. Phys. C **17**, 1563 (2006)
11. D. Shepard, *Proceeding of the 23rd ACM National Conference* (1968), p. 517
12. B. Chopard, M. Droz, *Cellular Automata and Modeling of Physical Systems* (Cambridge University Press, 1998), p. 353
13. D.A. Wolf-Gladrow, *Lattice-Gas Cellular Automata and Lattice Boltzmann Models: An introduction* (Springer, 2000), p. 308
14. D.L. Turcotte, G. Schubert *Geodynamics* (Cambridge University Press, 2002), p. 450
15. A. Bejan *Convection heat transfer* (Wiley, 2004), p. 450